



# A study of parameter and post-processing effects on surface quality improvement of Binder Jet 3D-printed Invar36 alloy parts

A. Lores<sup>1</sup> · N. Azurmendi<sup>1</sup> · I. Agote<sup>1</sup> · E. Espinosa<sup>2</sup> · M. B. García-Blanco<sup>2</sup>

Received: 12 May 2021 / Accepted: 12 January 2022 / Published online: 2 February 2022  
© The Author(s), under exclusive licence to Springer Nature Switzerland AG 2022

## Abstract

Binder Jetting Additive Manufacturing technology, besides its high-productivity manufacturing potential, it also offers a high accuracy fabrication route for less common metal alloys or special purpose applications. In the present work, Binder Jet 3D-printed Invar36 alloy parts' surface quality improvement is studied. Invar36 is a Fe–Ni alloy which presents near zero coefficient of thermal expansion below its curie temperature (279 °C) and it is widely used for high precision instrumentation in space environment. D90 < 22 µm grade Invar36 powder was used and printing process parameters were optimized following the Taguchi DoE methodology, to reduce sintered parts' surface roughness. Additional sandblasting and electropolishing operations were performed and part surface roughness was reduced from 5 µm Ra to 1.5 µm Ra. Near surface closed porosity emerged and enlarged during the electropolishing process, leaving a non-homogeneous surface appearance. Consequently, a Hot Isostatic Pressing (HIP) thermal treatment was applied to reduce part overall and near-surface porosity, reaching a relative density of 99.8%. After the sandblasting and electropolishing of HIP-ed parts, surface roughness was further reduced to 1 µm Ra maintaining and homogeneous and clean surface. The results of the study showed that Binder Jet 3D-printed Invar36 parts with low surface roughness can be obtained, getting this process and material closer to future space optics developments.

**Keywords** Binder jetting · Electropolishing · Invar36 · Surface roughness · Surface porosity · Additive manufacturing · Space

## 1 Introduction

Among all existing alloys, the Invar alloy family presents the lowest CTE below their curie temperature. This iron-nickel based alloys, present a superior dimensional stability (volume INVARIance) due to opposing effects of the expansion during the material heating and magnetorestriction effects of their microstructure [1]. The Invar36 alloy (Fe–36wt% Ni) is one of the most used one among the invar family. This alloy present excellent mechanic behaviour at cryogenic temperatures, but its ductility and low thermal conductivity makes it

difficult to be machined [1–3]. Due to these features, it has been widely used as a highly reliable precision material in components where high dimensional stability is required: thermal mismatch solving in PCB-ceramic joinings, main optic mirror clampings for dealing with mechanical interferences [4], secondary optics and refocusing mechanisms [5] and for the new James Webb space telescope backplane fittings and interfaces, for example.

One of the objectives of this study is to explore alternative processing routes for the manufacturing of parts for space, and more specifically those related with optical applications. Traditionally, machining processes have been used to fabricate optical mirrors from blank material, which has the detrimental effect of generating residual stresses [6]. Also, the machining process for very small and fine invar details, like the vane strips of the XMM observatory is indeed very challenging [7].

To this aim, Binder Jetting (BJ) Additive Manufacturing (AM) technology has been selected as an appropriate fabrication methodology for this alloy, which is an indicated AM

✉ A. Lores  
asier.lores@tecnalia.com

<sup>1</sup> Tecnia, Basque Research and Technology Alliance (BRTA), Mikeletegi Pasealekua 2, Parque Tecnológico de San Sebastián, 20009 Donostia-San Sebastián, Spain

<sup>2</sup> CIDETEC. Basque Research and Technology Alliance (BRTA), Po. Miramón 196, 20014 Donostia-San Sebastián, Gipuzkoa, Spain

processing technology for materials with low machinability and materials with challenging thermal properties for laser or electron beam based AM processes.

Binder jetting 3D-printing is a powder-bed based AM technology which employs a liquid binding agent for selectively join the powder particles of consecutively build powder layers [8]. The BJ process works as follows: first, the powder is deposited onto a platform by a powder dispenser system and then spreaded out by a roller or doctor blade forming a new powder layer. After that, one printhead selectively deposits the binder onto the powder-bed printing one section of the sliced CAD file of the part. This process is repeated until the entire part is printed. Then, the binder is cured to make the part consistent for handling purposes. Finally, the part is retrieved from the powder bed and subjected to a sintering cycle where the binder is burnt out and the part consolidates due to a metallurgical bonding of the powder particles.

The sintering of particulate materials printed with BJ technology usually involves the presence of porosity and difficulties to achieve full dense parts [9, 10]. Different approaches have been studied to obtain full density via BJ such as the use of bimodal mixtures [11–13], spray-dried granules [14], slurry based powders [15], sintering process (addition of sintering additives, liquid-phase sintering mechanism, pressure-assisted sintering, [9, 16, 17] etc.), among others.

On the other hand, in addition to the problem of porosity itself, it is well known that parts built by AM, and in this case by BJ, use to have a final poor surface quality due to stair step effect and due to powder particle surface bonding caused irregularities [18]. Also, the powder bed and sample porosity have a direct impact on the sample surface quality [19]. For some components, such as parts for space related optical applications, the modification of AM part surface is required to achieve a specific surface quality. The most common surface treatments reported in the literature for AM parts include mechanical treatments such as machining, grinding or blasting, laser treatments, and finally chemical and electrochemical processes [20]. For applications where residual stress need to be avoided, chemical or electrochemical treatments are usually the most recommended ones.

As the porosity and the difficulties of reaching full density materials are some of the major concerns of Binder Jetting technology, Hot Isostatic Pressure (HIP) thermal cycle has been considered for the present study. HIP is a thermal cycle where an inert gas is introduced isostatically pressing the introduced powder or already solid samples, to sinter and/or increase its density, by the dissolution of entrapped gas in the material matrix or on the material surface [21]. Although the main applications of HIP technique consist into the full density sintering of loose powder compacts, it also has been widely studied for full consolidation of

additively manufactured parts by various techniques, such as Selective Laser Melting [22–24], Electron Beam Melting [25–27] or Direct Metal Laser Sintering [28]. On the other hand, there are few studies up to date where the HIP technique is applied to Binder Jetted parts. The existing works have proved its value for sintered BJ sample density increase [29–31]. Nevertheless, a minimum of near 90% of initial relative density of the samples is required for a successful HIP treatment, as closed porosity is needed for the isostatic pressing of the samples [30].

Electropolishing (EP) is an electrochemical process that uses anodic dissolution to remove material in a controlled way, in which concentrated acid electrolytes are usually employed for metallic alloys [32]. However, different metals need different types of electrolytes and the properties of electrolyte directly affects the final EP effect [32]. The electropolishing of a wide range of different metal alloys, manufactured by AM or conventional manufacturing techniques, have been reported [33–36]. However, up to the authors knowledge, there is no literature available regarding the electropolishing process of Invar alloy parts produced by Binder Jetting technology.

In this context, this work has been focussed both on the printing process parameter optimization, and on the study of the electropolishing process effect over Binder Jetted invar 36 alloy parts, to reduce the surface roughness as a preliminary study for further space related application developments.

## 2 Materials and methods

### 2.1 Binder jetting of invar 36 alloy

Gas atomized Metal Injection Molding (MIM) Invar36 powder grade was selected for this study. The powder composition and particle size distribution provided by the supplier, Sandvik Osprey LTD, is shown in Table 1. Usually, spherical gas atomized MIM grade powders present a good balance between powder packability and flowability for Binder Jetting, which permits a wider range of processing parameter window together with a good sinterability and achievable densities [37]. SEM microscopy (Jeol JSM 5910 LV microscope with Oxford Inca 300 EDS accessory) was used to analyse the morphology of the powder particles and, Laser Diffraction (Malvern Mastersizer 2000) for measuring the Particle Size Distribution (PSD).

As the main objective of the present study is to reduce the surface roughness of the printed parts, a Fractional Factorial Design of Experiments (DoE) was performed selecting the most relevant printing parameters according to the literature [18, 38–40]. On the designed DoE, the effect that each process parameter has over the printed part surface quality was

**Table 1** Chemical composition and PSD of INVAR 36 powder supplied by Sandvik Osprey LTD

Chemical analysis (wt%)				
Fe	Ni	Mn	Si	C
Balanced	36.3	0.12	0.03	0.01
Particle size distribution ( $\mu\text{m}$ )				
D10	D50	D90		
5.8	12.3	21.9		

**Table 2** Selected study parameters and their levels for Taguchi experimental trial

	Level 1	Level 2	Level 3
<i>Study parameters</i>			
Saturation (%)	55	65	75
Recoat speed (mm/s)	60	70	80
Roller revolution (rpm)	300	450	600
Drying time (s)	10	15	20
<i>Fixed parameters</i>			
		Level	
Recoater vibration (rpm)		1900	
Layer thickness ( $\mu\text{m}$ )		50	
Roller traverse speed (mm/s)		3	

studied by means of ANOVA analysis, to select the most appropriate parameter levels. Taguchi methodology was followed, as it permits the analysis of multiple variables or parameters in a shorted experimental plan [41, 42]. In this case, a  $L_9$  ( $3^4$ ) orthogonal array was used to set up the experimental trials.

Table 2 shows the selected parameters of the study, which are the same parameter levels selected by a previous study performed by the authors [43], in which the effect of process parameters over the sample densities was studied. Each of the selected DoE factor or parameter drives one of each BJ printing stage: binder deposition (saturation), powder deposition (recoat speed), powder spreading (roller revolution) and binder drying (drying time). The selected parameter levels or values have been selected with the objective to have a stable process from which valuable defect-free samples can be obtained.

The fixed parameters were selected according to literature recommendations. A decrease of the powder-bed layer thickness seems to improve the surface finish of the part, and thus a 50  $\mu\text{m}$  layer thickness was selected according to [18]. It is remarkable that that powder particle size is usually lower than the half of the layer thickness according to the data of the literature [37]. On the other hand, the selection of low roller traverse speeds was done as it seems to increase part quality [9] and process robustness [44], as well as powder packing capabilities and surface quality [45].

In the same way than in the authors previous study [43], six rectangular samples of  $20 \times 20 \times 5$  mm were printed for each experimental trial using an ExOne Innovent BJ machine. The selected sample size responds to the need of having larger surface areas for surface roughness measurements. The curing of the green parts was performed at  $180^\circ\text{C}$  for 4 h, and then parts were sintered in a Carbolite GERO high vacuum furnace for 8 h at  $1140^\circ\text{C}$ . Sintered density was measured by Archimedes methodology using a Mettler AE 240 weight balance and isopropanol-2 as liquid medium.

## 2.2 Surface and morphology characterization

Surface roughness characterization was carried out using a Taylor-Hobson profilometer (Intra 50 mm model). The average value of standard surface roughness Ra (arithmetical mean) is reported according to the ISO 25178 standard. The measurements were performed on six random areas, three in  $x$  axes and three in  $y$  axes, per sample. The top surfaces of the printed samples were the selected ones for all the roughness measurements.

## 2.3 Surface treatments: blasting + electropolishing and further surface analysis

Sintered parts were blasted in two stages: firstly, in a Norblast' FN-30 T model blasting machine for 15 min, using corundum of 106–150  $\mu\text{m}$  particle size as the abrasive material and 5.5 bar air pressure, and placing the samples at 7–8 cm from the nozzle. Secondly, in a Norblast' S9 model blasting machine for 3 min, using round-shape glass microspheres of 40–70  $\mu\text{m}$  as the abrasive, 5.5 bar pressure and 5–6 cm sample-nozzle distance.

To clean blasted surfaces and to further reduce their surface roughness, an electropolishing process was performed. Electropolishing was carried out under a 0.75 A electrical current during 20 min, with a two-electrode system. Invar36 samples were set up as the anode and a stainless-steel foil as the cathode. Distance between electrodes was kept in 3 cm. Selected electrolyte was 100% ortho-phosphoric acid being the working temperature  $70^\circ\text{C}$ .

In addition to the surface roughness characterisation, the surface morphology of the treated samples was observed

using a ZEISS Ultra Plus field emission scanning electron microscope (FE-SEM). Confocal microscopy (Leica, Mod. DCM3D) was used to determine the sample profile and topography after electropolishing. Dye penetrant inspection (ARDROX-9813) was performed to characterize the surface porosity.

## 2.4 Hot isostatic pressing heat treatment

Some of the printed samples were subjected to a HIP thermal cycle, to further increase their density, prior to the surface roughness reduction treatments mentioned before. The HIP heat treatment was performed at 1100 °C and 100 MPa for 2 h in Argon using a heating rate of 10 °C/min and a cooling rate of 55 °C/min.

## 3 Results and discussion

### 3.1 Powder characterisation

The morphological analysis of powder particles carried out with SEM is shown in Fig. 1. As it can be observed, the powder particles are near-spherical in shape with some satellite particles attached, inherent to gas atomisation process. The powder section reveals the presence of pores entrapped within some particles, generated probably during the atomisation process [46]. The presence of both satellites and powder internal porosity may affect the optimal consolidation of AM parts [47].

As mentioned before, the increase of the packing density of the powder in Binder Jetting AM is desirable if high final sintered densities, better dimensional control and better surface quality is pursued [13, 48–50]. The Fig. 2 present the PSD curves of the acquired powder, which shows a limited fine particle content (<5 μm). Although the redesign of the raw material for, for example, adding higher fine particle

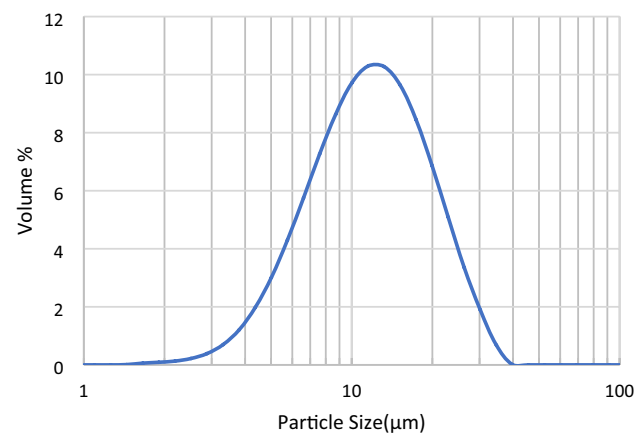


Fig. 2 PSD curve for the Invar 36 alloy powder used in the present study

content to enhance the sintering activity, or creating bimodal mixtures to increase the powder packing density, is one of the best options, this study is focussed on the reduction of surface roughness through the optimal process parameter level selection for a commercial grade invar36 powder.

### 3.2 Sintered part surface roughness and parameter optimization

Process parameter optimization was carried out by the study of the signal-to-noise ratios ( $S/N$ ) through Taguchi robust design methodology.  $S/N$  ratios of response variable were calculated for the “lower-is-better” quality characteristic with the following equation [19]:

$$S/N(\text{dB}) = -10 \log_{10} \left[ \frac{1}{n} \sum_{i=1}^n (R_{ai}^2) \right],$$

where  $R_{ai}$  is the  $i$ th surface roughness repetition for each trial conditions. Measured overall results for each manufacturing

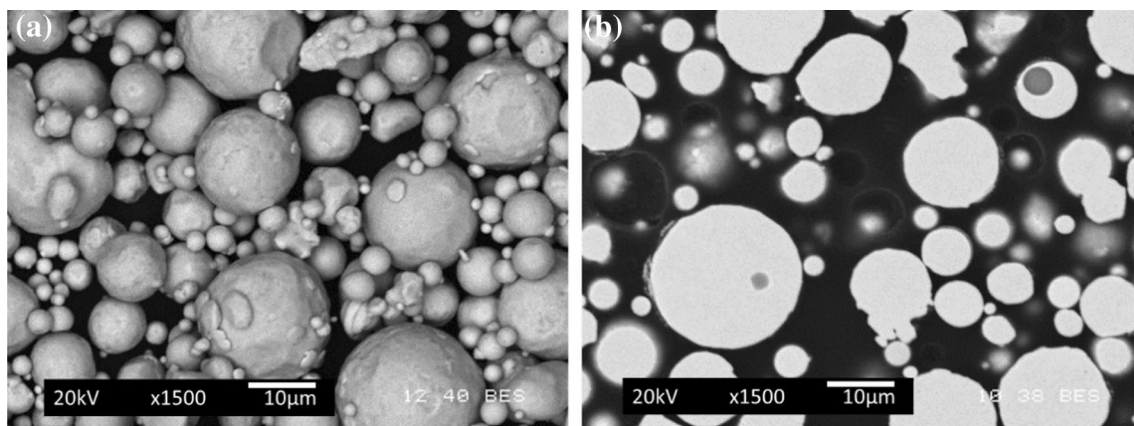


Fig. 1 SEM micrographs of **a** bulk Invar36 powder and **b** the cross section of some particles, showing entrapped porosity [43]

trial are summarized in the Table 3. As it can be seen, the overall top surface  $R_a$  of the sintered parts range between 5.29 and 7.53  $\mu\text{m}$ , and the sintered densities between 90 and 93%, in function of the manufacturing trial.

The ANOVA table and the process parameter effect on surface roughness reduction are shown in Table 4 and Fig. 3, respectively.

The results from ANOVA table indicate that the drying time has the mayor influence (51.1%) on the decrease of the final part surface roughness. It has been found that larger drying times increase the surface roughness. The binder saturation, with an initial contribution of 6% to result variation,

was pooled as an error term. In this particular study, where no columns of the  $L_9$  OA were left in Blanc, it is compulsory to assign one or more parameters as error terms, to have statistical significance of the computed results. This being the case, the  $F$  values of the ANOVA for all studied parameters, except for the drying time, were below 90% confidence level. Therefore, the interpretation of the parameter main effects must be handled with care due to the lack of high statistical significance.

The interpretation of the parameter effects shown in Fig. 3, can be divided according to the influence that each printing stage (powder layer building, binder deposition and

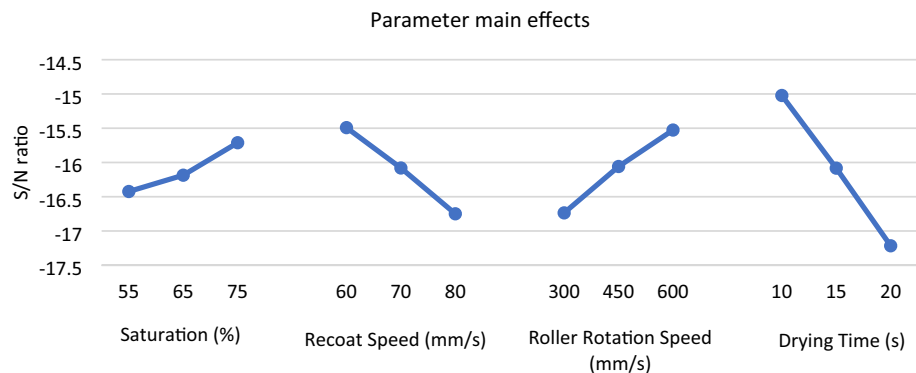
**Table 3** Results of surface roughness, standard deviation and  $S/N$  ratios for each experimental trial

Factors	Saturation		Recoat speed	Roller RPM	Drying time	Average $R_a$ ( $\mu\text{m}$ )	Average relative density (%)	$S/N$ ratios for surface roughness
	1	2						
Trials	1	1	1	1	1	5.85	93.1	-15.35
	2	1	2	2	2	6.52	91.9	-16.32
	3	1	3	3	3	7.53	91.4	-17.59
	4	2	1	2	3	6.77	91.5	-16.63
	5	2	2	3	1	5.29	92.6	-14.49
	6	2	3	1	2	7.43	91.5	-17.43
	7	3	1	3	2	5.27	92.0	-14.49
	8	3	2	1	3	7.40	90.6	-17.42
	9	3	3	2	1	5.76	92.4	-15.22

**Table 4** ANOVA table computed from calculated  $S/N$  ratios

Source of variation	DOF	Sum of squares, $S$	Variance, $V$	Variance Ratio, $F$	Pure sum of squares, $S'$	Percent contribution, $P$
Saturation	(2)	0.79	pooled			
Recoat speed	2	2.37	1.18	3.01	1.58	12.61
Roller RPM	2	2.20	1.10	2.79	1.41	11.23
Drying time	2	7.22	3.61	9.16	6.43	51.10
Error ( $e$ )	2	0.79	0.39	1	0	25.05
Total	8	12.59	-	-	-	100

**Fig. 3** Process parameter level main influence in part surface roughness



layer drying) has in the built part. It is worth mentioning that the optimization of the process has been performed inside the selected parameter range. Carefully looking to the Fig. 3 graph one can deduce that a more effective parameter levels may exist, as the parameter effect curves do not present maximum points for the studied levels.

On one hand, according to the present study results shown in Fig. 3, lower recoater speed (which means more deposited powder for each layer building) and higher roller rotation speed, decrease surface roughness. These results are in line with results reported in the literature. The higher roller rotation speed enhances the powder flowability, enabling a better layer packing and surface quality [51]. Additionally, according to mathematical modelling simulations [52] and experimental tests [39], the increasing of the powder feed thickness/powder layer thickness ratio seems to increase the powder packing rate due to the onset of some compaction forces perpendicular to the powder spreading direction.

On the other hand, according to Fig. 3, the surface roughness of the part seems to decrease with the increase of binder saturation. Too low saturation levels could not permit the proper bonding between powder particles, promoting the detachment of some powder particles during the consequent powder layer building, generating groove and defects and thus decreasing surface quality [18]. Additionally, too high saturation levels could promote part swelling [18] and particle gluing to the roller due to binder excess. Thus, it is of great importance to find an optimum saturation level that improves final part quality, which is subjected to the binder-powder system capillary pressure or saturation equilibrium [53].

The optimum saturation level can be tuned or adjusted with the layer drying or powder-bed heating step. As it can be seen in the results, the effect of the powder-bed drying over the result variation is much higher than the saturation effect, meaning that for a certain binder saturation level, the selection of the appropriate drying conditions is more crucial. As explained by [54], the effective binder saturation level that the powder layer has is lower than the selected print saturation, due to the partial evaporation of the solvent by the heat lamp or powder-bed heating system. There are some works that study the optimum or equilibrium binder saturation conditions by means of simulation or experimental procedures for certain powder systems as well as the binder drop and powder-bed interaction [53, 55–60]. None of them introduces the drying time or heating factor, which has been found to be influential for controlling the density and dimensions of the green parts [18, 43], and as explained before, it has a direct impact on the real saturation equilibrium of the powder bed/binder system. Therefore, there is a real need for further studies and deeper understanding of the effect of the drying step over the binder behaviour and its saturation equilibrium.

According to the results of the present study, the increase of the drying time leads to an increase of the surface roughness, this is, the increase of the transferred heat promotes less surface quality. As hypothesized by the authors, an excessive amount of heat accelerates the rapid surface evaporation of the deposited binder, changing the capillary pressure equilibrium and inducing a tensional state that can modify the arrangement of some particles. Those particle agglomerations will thus lead to the generation of cracks, which would be difficult to further close during the sintering step, affecting the surface quality of the final parts. The scheme of this process is shown in Fig. 4.

This cracking effect has been extensively studied in hydrogeology [61–66]. The surface crack formation and propagation is a common consequence of the desiccation of water saturated soils. The water evaporation induced capillary suction indeed has been found to be one of the main factors for the initiation of cracks in different soils and concrete systems [67, 68]. Despite the differences in particle sizes and compositions between soils and metal powders, the physical phenomenon occurring in both cases are very similar.

Additionally, the successive creation of cracks layer after layer can have an additional impact on the final density of the parts. As it can be seen in Fig. 5, the increase of drying time decreases both the surface quality and the final density of the parts.

Following the Taguchi methodology, estimated performance and its confidence interval at optimum parameter conditions (Table 5) is  $4.91 \pm 0.83 \mu\text{m Ra}$ . A confirmation test was run using the optimised process parameter levels. Achieved Ra was  $4.62 \mu\text{m}$  with a standard deviation of  $0.26 \mu\text{m}$ , which is within expected performance value range. The average final relative density of the optimum samples was 91.45%.

Once the printing process was optimized, additional samples were manufactured with the optimum parameter levels for further surface processing operations, with the objective of achieving a better surface quality.

### 3.3 Surface roughness reduction

As it was explained before, invar 36 printed and sintered samples were sand blasted and then electropolished to decrease their initial surface roughness. The sintered part initial surface roughness was  $5 \mu\text{m Ra}$ . Sand blasting reduced the surface roughness by 55%, and the later electropolishing process further reduced the surface roughness achieving an overall surface roughness decrease of 70%. Figure 6 shows the morphology of as-built, blasted and electropolished surfaces.

As it can be observed, as-built samples (Fig. 6a) show the typical wavy-like sintering irregularities on the sample top surface. Blasting media removes those

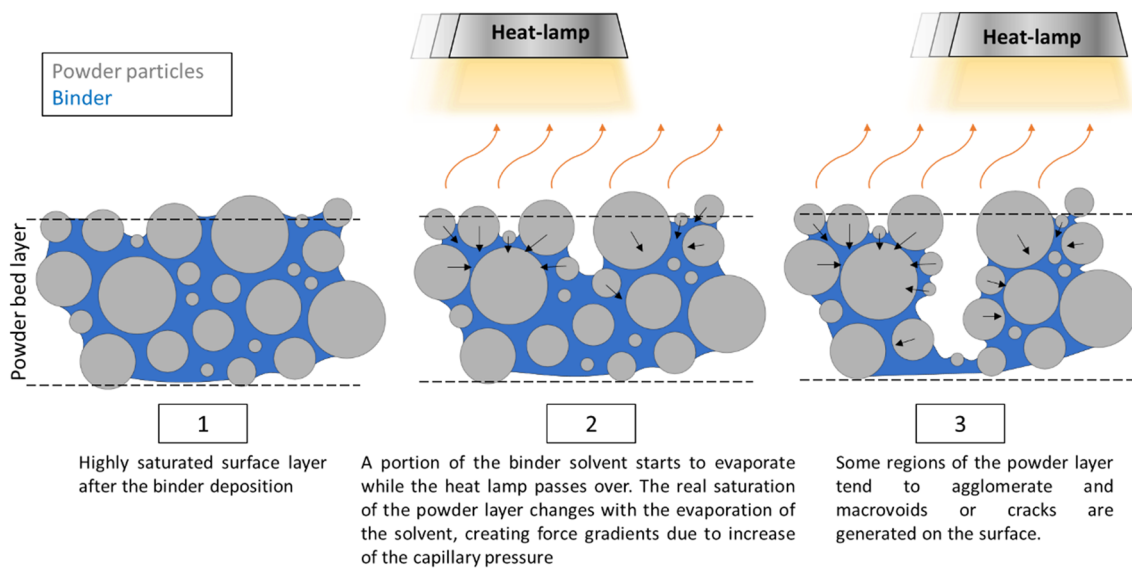


**Fig. 4** Surface crack formation effect due to the capillary action by drying the deposited binder

**Fig. 5** Relation between obtained part surface roughness (Ra) and relative sintered densities

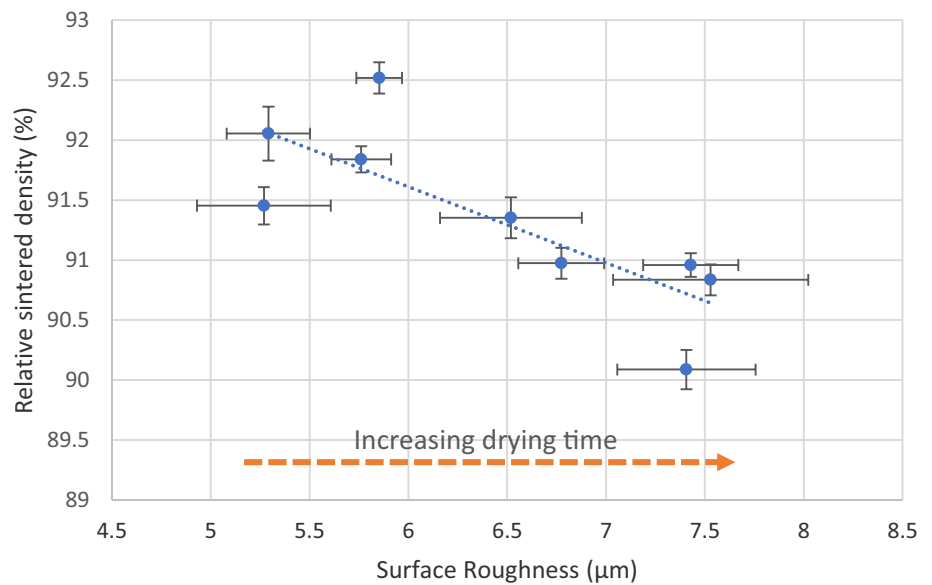


**Table 5** Optimum parameter conditions for surface roughness reduction

Parameter	Saturation (%)	Recoat speed (mm/s)	Roller rotation (rpm)	Drying time (s)
Level	75	60	600	10

irregularities and a more homogeneous textured surface is obtained. After the electropolishing process, a much smoother surface is achieved. However, some pores came out on the treated surface. Additionally, there were some areas where there was higher open pore concentration.

This higher pore concentration areas were directly visible, and they appeared forming some concentric marks on the top surface of the samples, as can be seen in Fig. 7. The distribution of those marks varied from sample to sample, and in some ones, they were more appreciable than in others.

A deeper analysis of the surface morphology by SEM imaging, shown in Fig. 8, revealed more in detail those higher pore concentration areas. The blue lines on Fig. 8 delimit the boundaries of those areas.

The porosity of these surfaces was also confirmed by penetrant dye testing. Figure 9 shows a blasted sample and two electropolished samples before and after the application of

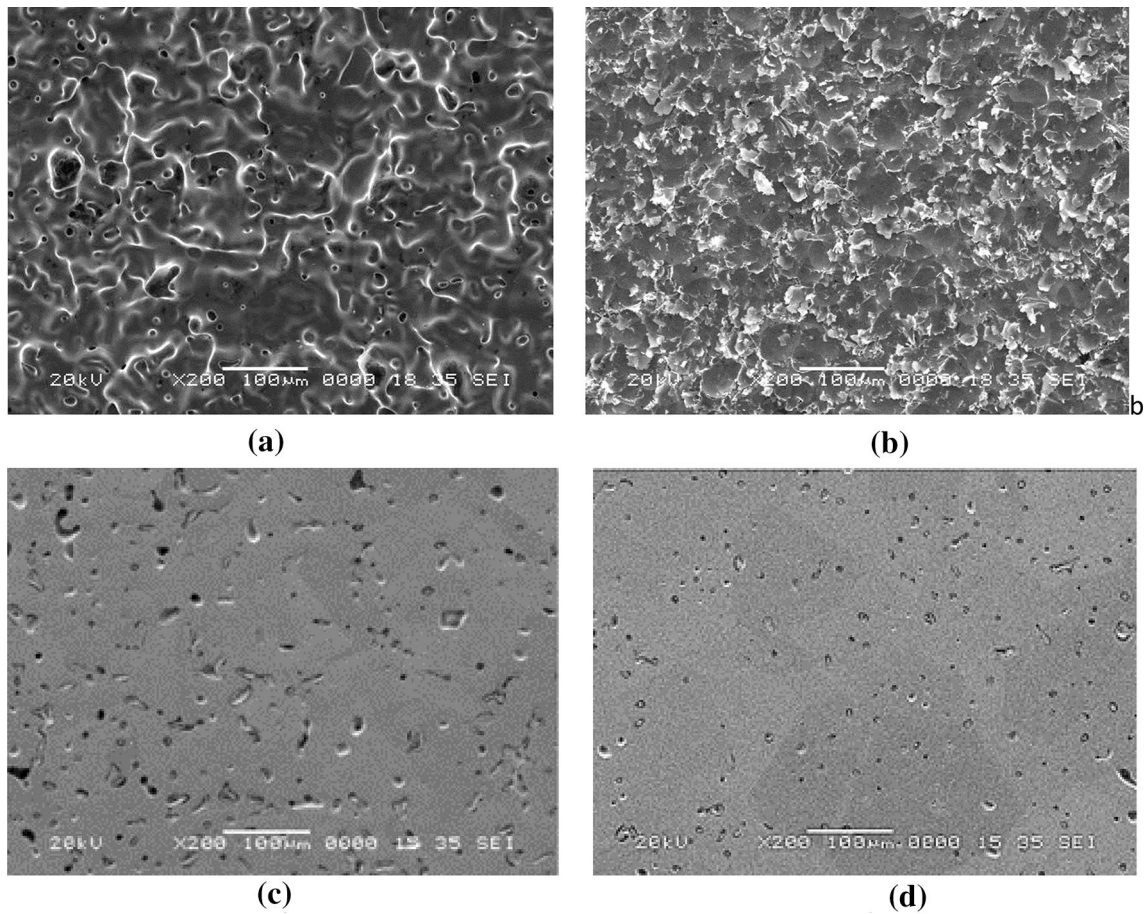


**Fig. 6** FESEM images of **a** as-built surface, **b** blasted surface and **c, d** electropolished surfaces in two different areas of the same sample

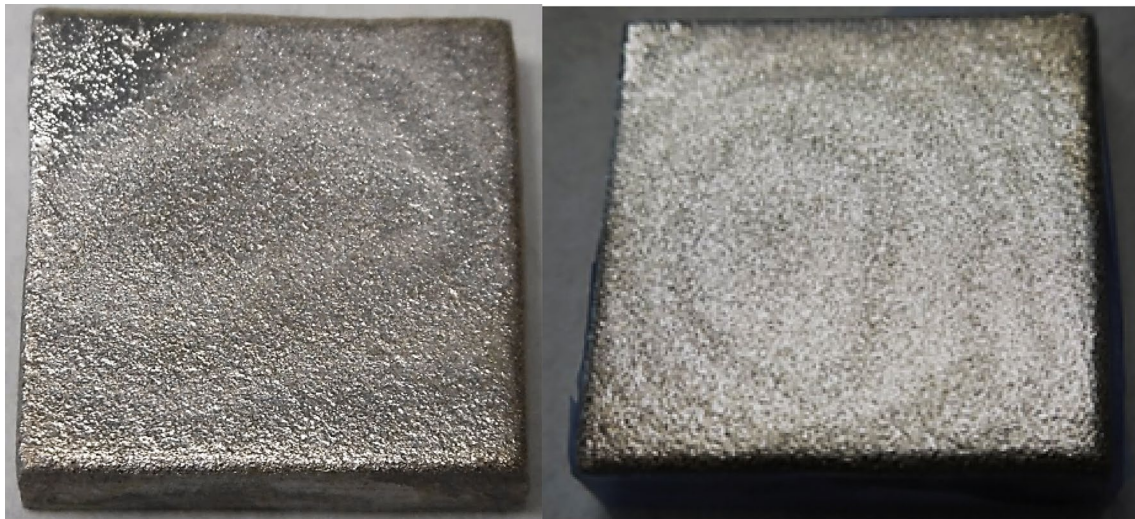


**Fig. 7** Images of two electropolished samples with math concentric marks

Penetrant Liquid. Blasted surface did not show any significant defect while both electropolished surfaces, presented these concentric marks with higher pore density.

To discard that these marks were produced by the electropolishing process, some as-built samples were also polished mechanically. Figure 10 shows an image of the



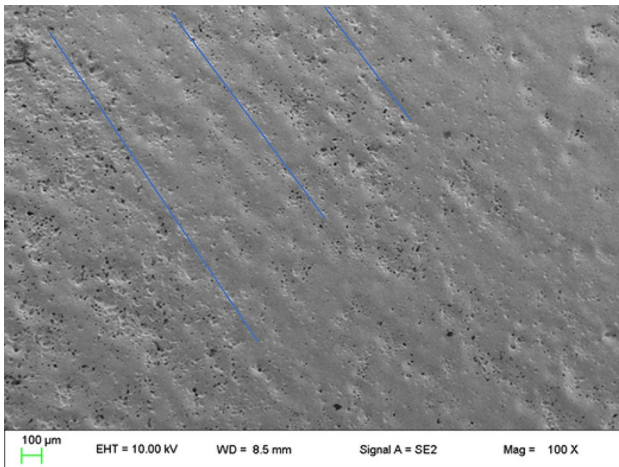


**Fig. 8** FESEM micrograph of an electropolished surface where different zones with high pore density could be observed

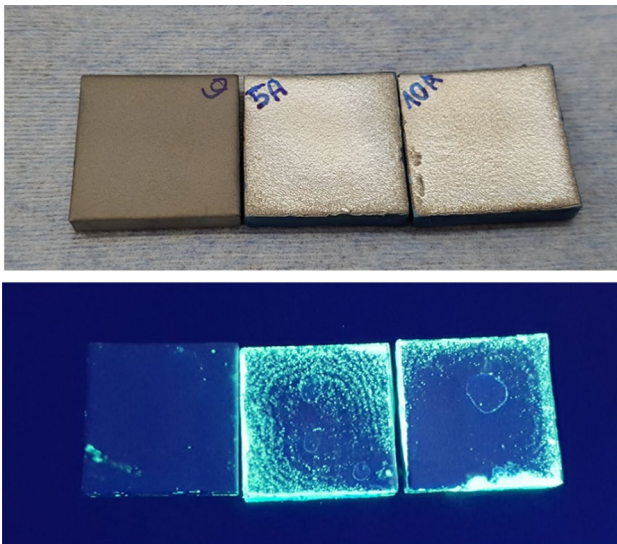


**Fig. 9** Images of a blasted sample and two electropolished 17×17 mm samples before and after Penetrant Liquid test

mechanically polished sample and as it can be observed, the porous marks still appeared on the surface, confirming that they come from the sintered sample.

Moreover, it was observed that after the electropolishing process the surface flatness was modified, unlike it usually happens with electropolished samples produced by other manufacturing processes. Electropolished Binder Jetting samples became concave. Figure 11 presents the confocal image and profile obtained for these electropolished parts.

This behaviour could be related to the internal porosity of the samples. Samples produced by this technology have a non-homogeneous internal porosity distribution, which is more concentrated on the superficial area of the samples, and

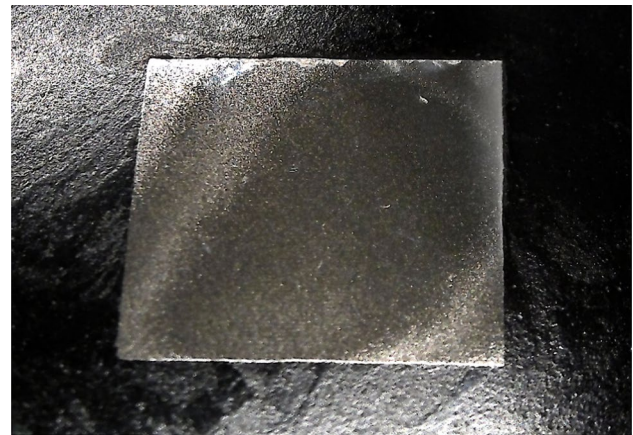


**Fig. 10** Image of a mechanically polished Invar36 sample with 17 mm of side lengths

between the built powder layers [69]. The obtained results suggest that the surface roughness and aspect after electropolishing is affected by the internal porosity structure near the surface of the samples. Electropolishing oxidises or dissolves the elements on the surface homogeneously until internal pores that are near the surface or between the layers are reached. When those pores appear, the electropolishing electric current density could increase near the pore-edges and could enlarge them rather than further wear the surface out. The sample areas with less pore density, for example on the surface centre, continues electropolishing producing the concave structure. The Fig. 12 shows an illustrative scheme of the concavity issue and pore distribution in Binder jet 3D printed and sintered samples.

Additionally, regarding the pore marks that also appeared on the mechanically polished samples, some pore interlayers were revealed due to the partial warpage of the sample corners during the sintering process, as it can be seen on the sintered part cross section shown in Fig. 13.

In this context, to obtain a homogeneous and flat surface after the electropolishing of Binder Jetted samples, the part internal porosity must be eliminated. For this purpose, HIP treatment was applied to some sintered samples. Obtained sample density after HIP postprocessing was  $99.83 \pm 0.01\%$ .

Surface roughness and morphology of HIP samples were measured and analysed, and compared with the previous ones, as can be seen on Fig. 13. As it can be observed, surface roughness slightly increased after HIP and the marks still were visible. Further blasting and electropolishing treatments were applied to HIP-ed samples, to remove the remaining open porosity of the surface. A further surface roughness decrease was observed, and the surface appeared brighter without any apparent porosity marks.

These results suggest that blasting and electropolishing processes were able to correctly smooth the treated part

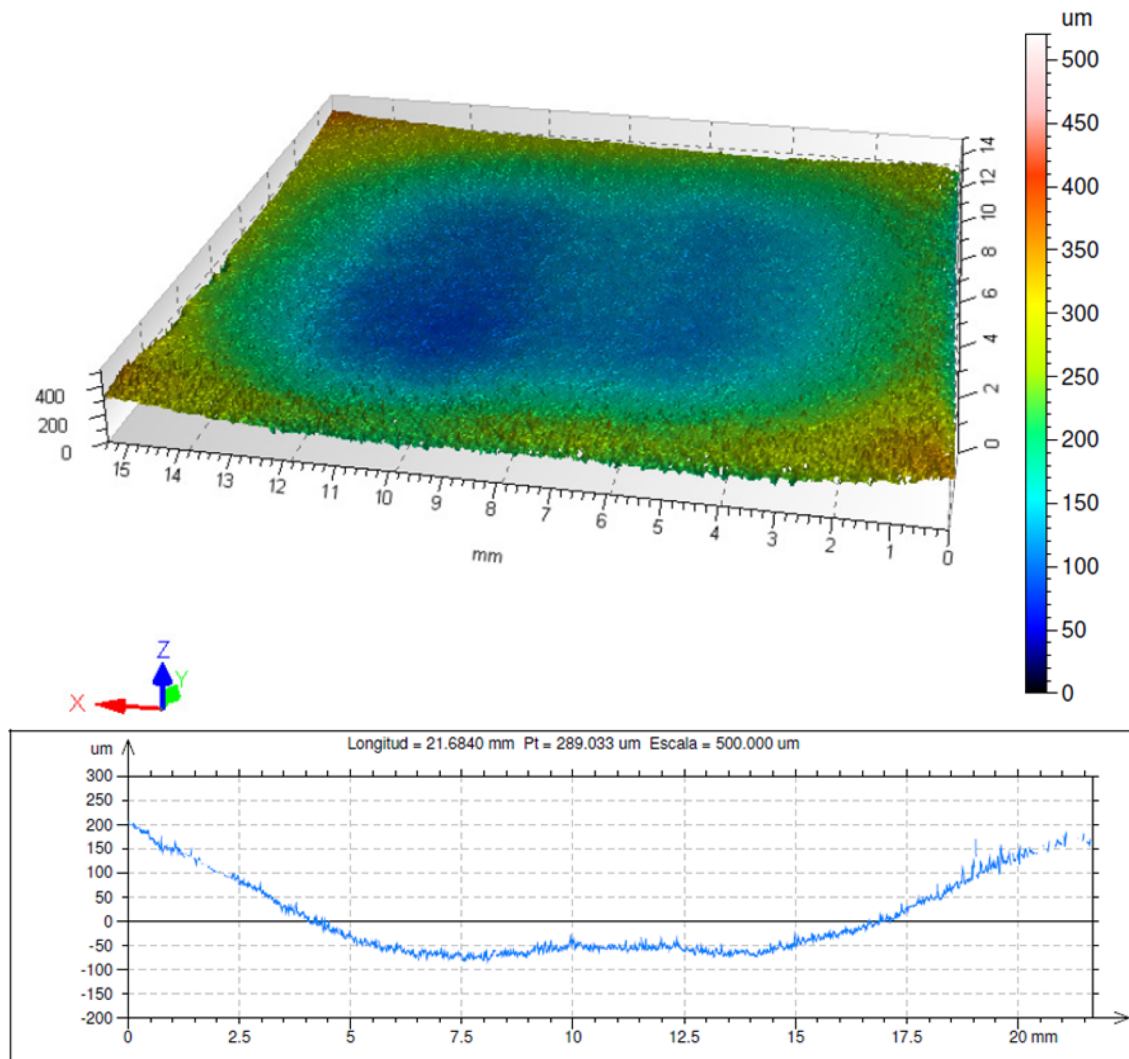


**Fig. 11** Confocal image and profile of an electropolished Invar36 sample

surface. Since the part porosity was previously closed by the HIP process, no marks appeared on the treated surfaces after blasting and electropolishing, and a surface roughness of  $1 \mu\text{m Ra}$  was reached.

The sample cross section and surface analysis before and after the HIP treatment was also carried out by FESEM (Fig. 14). Obtained micrographs showed that the HIP was able to eliminate nearly all the porosity, and consequently the concentric marks of the as-sintered samples.

## 4 Conclusions

The present work studies the different aspects of surface quality improvement for binder jet 3D-printed invar36 alloy parts, to evaluate the viability of the alloy and the process

for potential space optical applications. The main results and conclusions of the present study are:

- $1 \mu\text{m Ra}$  surface roughness can be reached with the binder jetting process optimization and subsequent HIP treatment, sandblasting and electropolishing operations.
- According to the results, the binder drying time has a major impact on the reduction of the surface roughness comparing to other printing parameters, probably due to the capillary force induced crack generation during the drying step.
- Electropolishing and sandblasting operations performed to Binder Jet 3D printed and sintered samples decrease the surface roughness from  $5 \mu\text{m Ra}$  to  $1.5 \mu\text{m Ra}$ . However, the obtained surfaces do not have a homogeneous appearance due to surface treatment induced porosity enlargement and varies from tested part to part. This

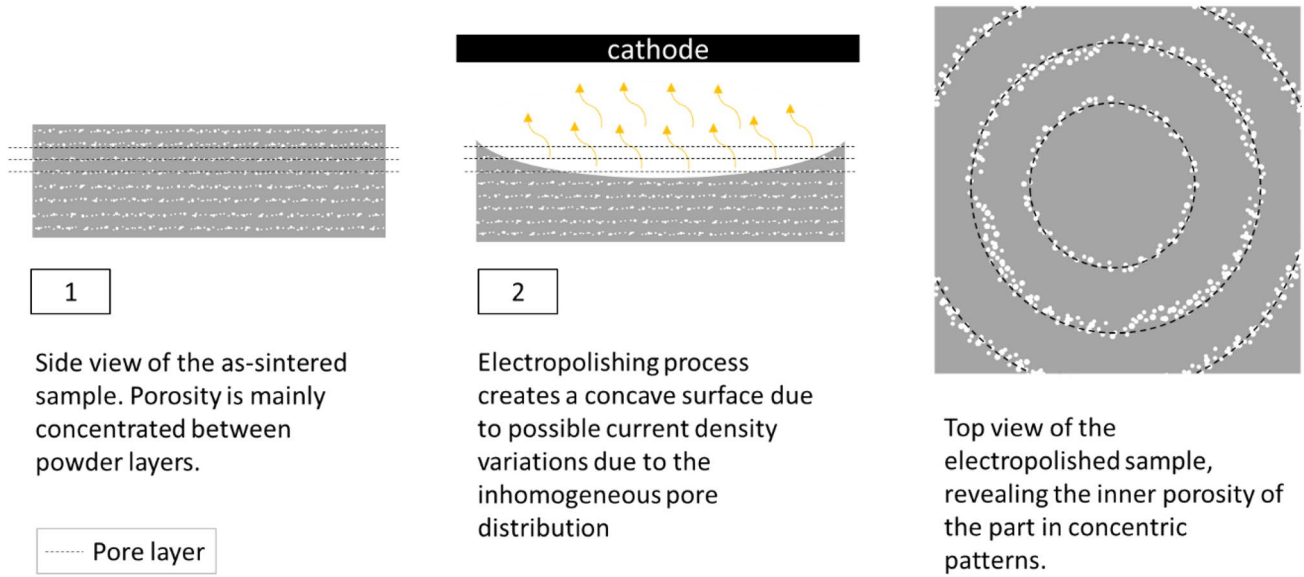
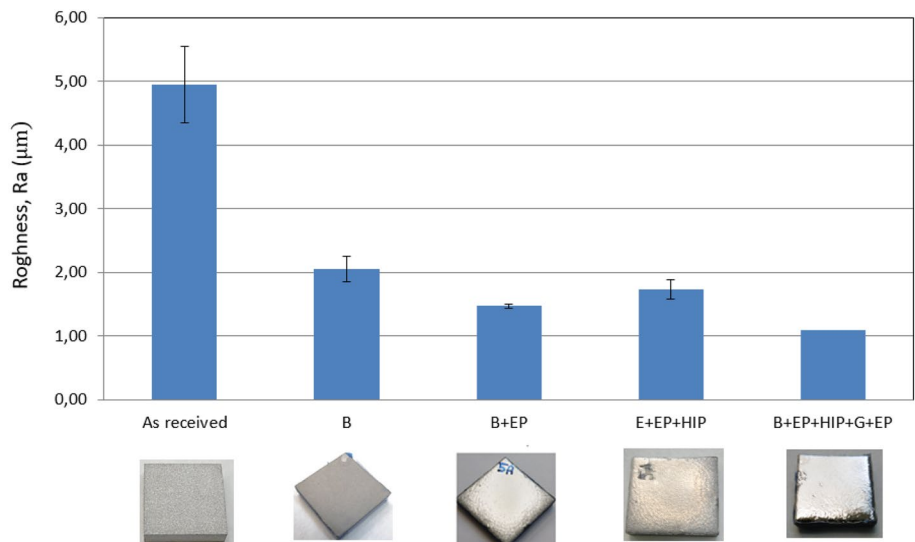


**Fig. 12** Scheme showing the Binder jet 3D printed and sintered sample internal porosity distribution and concavity issue after the electropolishing process

**Fig. 13** Surface roughness of Invar36 material as-built and after different postprocessing treatments (B: blasting, EP: electropolishing, and HIP)



inhomogeneity effect has been linked to the near-surface pore concentration on sintered binder jetting samples.

- HIP thermal treatment almost eliminated the part porosity, increasing the part relative density to a 99.8%. HIP treated, sandblasted and electropolished parts showed a homogeneous surface with a surface roughness of 1 μm Ra.

Further studies will investigate the optimization of the electropolishing process for additional surface roughness reduction of invar36 samples. Also, the complex shaped part manufacturing potential of binder jetting process will be studied, together with the additional post-processing techniques, to validate the ability of the whole process chain to manufacture next generation light weighted parts for space applications.

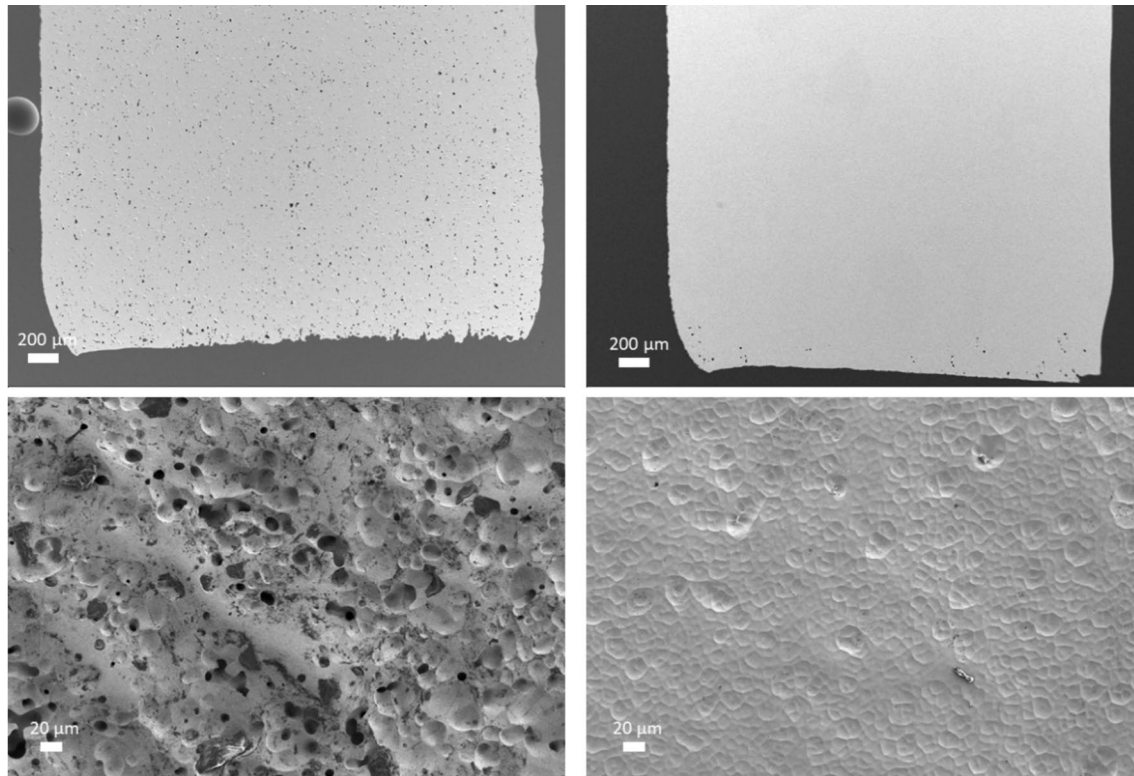


**Fig. 14** FESEM micrographs of cross section and surfaces of blasted + electropolished surfaces before (left) and after (right) HIP treatment

**Acknowledgements** The authors want to kindly acknowledge the CEIT-BRTA centre for the help provided with the HIP treatment of the samples used in this study.

**Funding** This article was funded by Ministerio de Ciencia, Innovación y Universidades (Grant nos: SURF-ERA, EXP-00137314/ CER-20191003, M. Belén García), Eusko Jaurlaritza (Grant no. ELKARTEK ADDISEND KK-2018/00115, Asier Lores).

## References

- Hidalgo J, Jiménez-Morales A, Gelin JC, Torralba JM (2014) Mechanical and functional properties of Invar alloy for  $\mu$ -MIM. *Powder Metall* 57(2):127–136
- Guillaume CE (1904) Invar and its applications. *Nature* 71(1832):134–139
- Qiu C, Adkins NJE, Attallah MM (2016) Selective laser melting of Invar 36: Microstructure and properties. *Acta Mater* 103:382–395
- IPC-THAG (2019) Technologies for optical passive instruments (mirrors). European Space Technology Harmonisation Technical Dossier
- Janu P, Neugebauer C, Plank H, Strube B (2017) Refocusing mechanism for meteorat 3rd generation. *Proc. ESMATS 2017*, pp 20–22
- Paquin RA (2019) *Metal Mirrors*. Handbook optomechanical engineering. CRC Press, Boca Raton, pp 89–110
- De Chambure D, Lainé R, Van Katwijk K, Kletzkine P (1999) XMM's X-ray telescopes. *ESA bulletin n°100* - December 1999
- ASTM F2792-12a (2013) Standard terminology for additive manufacturing technologies
- Zhang S, Miyajagi H, Yang L, Ali Zandinejad A, Dilip J, Stucker B (2014) An experimental study of ceramic dental porcelain materials using a 3D print (3DP) process. In: *Solid Free. Fabr. Symp.*, pp 991–1011
- Chou D-T, Wells D, Hong D, Lee B, Kuhn H, Kumta PN (2013) Novel processing of iron–manganese alloy-based biomaterials by inkjet 3-D printing. *Acta Biomater* 9(10):8593–8603
- Do T, Kwon P, Shin CS (2017) Process development toward full-density stainless steel parts with binder jetting printing. *Int J Mach Tools Manuf* 121:50–60
- Verlee B, Dormal T, Lecomte-Beckers J (2012) Density and porosity control of sintered 316L stainless steel parts produced by additive manufacturing. *Powder Metall* 55(4):260–267
- Bai Y, Wagner G, Williams CB (2015) Effect of bimodal powder mixture on powder packing density and sintered density in binder jetting of metals. In: *2015 Annu. Int. Solid Free. Fabr. Symp.*, p 62
- Williams CB, Cochran JK, Rosen DW (2011) Additive manufacturing of metallic cellular materials via three-dimensional printing. *Int J Adv Manuf Technol* 53(1–4):231–239
- Holman RK (2001) Effects of the polymeric binder system in slurry-based three dimensional printing of ceramics. Massachusetts Institute of Technology
- Gaytan SM et al (2015) Fabrication of barium titanate by binder jetting additive manufacturing technology. *Ceram Int* 41(5):6610–6619
- Orange MJ, Kuhn HA, Knor PP, Lizzi T (2015) Process for making nickel-based superalloy articles by three-dimensional printing. *WO 2015/183796 A1*
- Chen H, Zhao YF (2016) Process parameters optimization for improving surface quality and manufacturing accuracy of

- binder jetting additive manufacturing process. *Rapid Prototyp J* 22(3):527–538
19. Shakor P, Nejadi S, Paul G, Sanjayan J (2020) Dimensional accuracy, flowability, wettability, and porosity in inkjet 3DP for gypsum and cement mortar materials. *Autom Constr* 110:102964
  20. Lee JY, Nagalingam AP, Yeo SH (2021) A review on the state-of-the-art of surface finishing processes and related ISO/ASTM standards for metal additive manufactured components. *Virtual Phys Prototyp* 16(1):68–96
  21. Atkinson HV, Davies S (2000) Fundamental aspects of hot isostatic pressing: an overview. *Metallurgical Mater Transact* 31A:2981–3000
  22. Kasperovich G, Hausmann J (2015) Improvement of fatigue resistance and ductility of TiAl6V4 processed by selective laser melting. *J Mater Process Technol* 220:202–214
  23. Leuders S, Lienen T, Lammers S, Tröster T, Niendorf T (2014) On the fatigue properties of metals manufactured by selective laser melting—the role of ductility. *J Mater Res* 29(17):1911–1919
  24. Leuders S et al (2013) On the mechanical behaviour of titanium alloy TiAl6V4 manufactured by selective laser melting: fatigue resistance and crack growth performance. *Int J Fatigue* 48:300–307
  25. Murr LE et al (2011) Microstructural architecture, microstructures, and mechanical properties for a nickel-base superalloy fabricated by electron beam melting. *Metall Mater Trans A* 42(11):3491–3508
  26. Sames WJ, Unocic KA, Dehoff RR, Lolla T, Babu SS (2014) Thermal effects on microstructural heterogeneity of Inconel 718 materials fabricated by electron beam melting. *J Mater Res* 29(17):1920–1930
  27. Mohammadhosseini A, Fraser D, Masood SH, Jahedi M (2013) Microstructure and mechanical properties of Ti–6Al–4V manufactured by electron beam melting process. *Mater Res Innov*. <https://doi.org/10.1179/1432891713Z.000000000302>
  28. Mower TM, Long MJ (2016) Mechanical behavior of additive manufactured, powder-bed laser-fused materials. *Mater Sci Eng A* 651:198–213
  29. Kernan BD, Sachs EM, Oliveira MA, Cima MJ (2007) Three-dimensional printing of tungsten carbide-10 wt% cobalt using a cobalt oxide precursor. *Int J Refract Met Hard Mater* 25(1):82–94
  30. Kumar AY, Bai Y, Eklund A, Williams CB (2018) The effects of Hot Isostatic Pressing on parts fabricated by binder jetting additive manufacturing. *Addit Manuf* 24:115–124
  31. Kumar A, Bai Y, Eklund A, Williams CB (2017) Effects of hot isostatic pressing on copper parts fabricated via binder jetting. *Procedia Manuf* 10:935–944
  32. Landolt D (1987) Fundamental aspects of electropolishing. *Electrochim Acta* 32(1):1–11
  33. Simson T, Emmel A, Dwars A, Böhm J (2017) Residual stress measurements on AISI 316L samples manufactured by selective laser melting. *Addit Manuf* 17:183–189
  34. Urlea V, Brailovski V (2017) Electropolishing and electropolishing-related allowances for IN625 alloy components fabricated by laser powder-bed fusion. *Int J Adv Manuf Technol* 92(9–12):4487–4499
  35. Han W, Fang F (2019) Fundamental aspects and recent developments in electropolishing. *Int J Mach Tools Manuf* 139:1–23
  36. Tyagi P et al (2019) Reducing the roughness of internal surface of an additive manufacturing produced 316 steel component by chempolishing and electropolishing. *Addit Manuf* 25:32–38
  37. Lores A, Azurmendi N, Agote I, Zuza E (2019) A review on recent developments in binder jetting metal additive manufacturing: materials and process characteristics. *Powder Metall* 62(5):267–296
  38. Hsu TJ, Lai WH (2010) Manufacturing parts optimization in the three-dimensional printing process by the Taguchi method. *J Chin Inst Eng Trans Chin Inst Eng A* 33(1):121–130
  39. Shrestha S, Manogharan G (2017) Optimization of binder jetting using Taguchi method. *Jom* 69(3):491–497
  40. Wang Y, Zhao YF (2017) Investigation of sintering shrinkage in binder jetting additive manufacturing process. *Procedia Manuf* 10:779–790
  41. Roy RK (2010) A primer on The Taguchi method
  42. Box GEP (2009) *Statistics for experimenters design, innovation, and discovery*. Wiley, Oxford
  43. Azurmendi N, Lores A, Guraya C, Agote I (2020) Binder jetting of high dimensional stability alloy for space applications. In: *Euro PM 2018 Congr. Exhib*
  44. Sheydaei E, Fishman Z, Vlasea M, Toyserkani E (2017) On the effect of throughout layer thickness variation on properties of additively manufactured cellular titanium structures. *Addit Manuf* 18:40–47
  45. Haeri S, Wang Y, Ghita O, Sun J (2017) Discrete element simulation and experimental study of powder spreading process in additive manufacturing. *Powder Technol* 306:45–54
  46. Rabin BH, Smolik GR, Korth GE (1990) Characterization of entrapped gases in rapidly solidified powders. *Mater Sci Eng A* 124(1):1–7
  47. Anderson IE, White EMH, Dehoff R (2018) Feedstock powder processing research needs for additive manufacturing development. *Curr Opin Solid State Mater Sci* 22(1):8–15
  48. German RM (1989) *Particle packing characteristics*. Metal Powder Industries Federation
  49. Sohn HY, Moreland C (1968) The effect of particle size distribution on packing density. *Can J Chem Eng* 46(3):162–167
  50. Lanzetta M, Sachs E (2003) Improved surface finish in 3D printing using bimodal powder distribution. *Rapid Prototyp J* 9(3):157–166
  51. Zhang W, Mehta A, Desai PS, Fred Higgs III C (2017) Machine learning enabled powder spreading process map for metal additive manufacturing (Am), pp 1235–1249
  52. Shanjani Y, Toyserkani E (2008) Material spreading and compaction in powder-based solid freeform fabrication methods: mathematical model. *International Solid Freeform Fabrication Symposium*, pp 399–410
  53. Miyajima H, Yang L (2016) Equilibrium saturation in binder jetting additive manufacturing processes: theoretical model vs. experimental observations. In: *Solid freeform fabrication symposium—additive manufacturing, vol I*, pp 1945–1959
  54. Crane NB (2020) Impact of part thickness and drying conditions on saturation limits in binder jet additive manufacturing. *Addit Manuf* 33:101127
  55. Miyajima H, Zhang S, Yang L (2018) A new physics-based model for equilibrium saturation determination in binder jetting additive manufacturing process. *Int J Mach Tools Manuf* 124:1–11
  56. Oostveen MLM, Meesters GMH, van Ommen JR (2015) Quantification of powder wetting by drop penetration time. *Powder Technol* 274:62–66
  57. Hapgood KP, Litster JD, Biggs SR, Howes T (2002) Drop penetration into porous powder beds. *J Colloid Interface Sci* 253(2):353–366
  58. Nefzaoui E, Skurtys O (2012) Impact of a liquid drop on a granular medium: inertia, viscosity and surface tension effects on the drop deformation. *Exp Therm Fluid Sci* 41:43–50
  59. Tan H (2016) Three-dimensional simulation of micrometer-sized droplet impact and penetration into the powder bed. *Chem Eng Sci* 153:93–107
  60. Barui S et al (2020) Probing ink-powder interactions during 3D binder jet printing using time-resolved X-ray imaging. *ACS Appl Mater Interfaces* 12(30):34254–34264

61. Bordoloi S, Ni J, Ng CWW (2020) Soil desiccation cracking and its characterization in vegetated soil: a perspective review. *Sci Total Environ* 729:138760
62. Peron H, Laloui L, Hu LB, Hueckel T (2013) Formation of drying crack patterns in soils: A deterministic approach. *Acta Geotech* 8(2):215–221
63. Morris PH, Graham J, Williams DJ (1992) Cracking in drying soils. *Can Geotech J* 29(2):263–277
64. Chertkov VY, Ravina I (2002) Combined effect of interblock and interaggregate capillary cracks on the hydraulic conductivity of swelling clay soils. *Water Resour Res* 38(8):32-1-32–15
65. Shaughnessy BO, Vavylonis D (2000) Interfacial reaction kinetics. *Phys J E* 177:159–177
66. Atique A, Sanchez M (2011) Analysis of cracking behavior of drying soil. *Int Conf Environ Sci Technol* 6:66–70
67. Tang CS, Shi B, Liu C, Gao L, Inyang HI (2011) Experimental investigation of the desiccation cracking behavior of soil layers during drying. *J Mater Civ Eng* 23(6):873–878
68. Schmidt M, Slowik V (2009) Capillary shrinkage cracking and its prevention by controlled concrete curing. In: *Proc. 2nd Int. RILEM Work. Concr. Durab. Serv. Life Plan. – Concr.*, no 1, p 8
69. Kumar AY, Wang J, Bai Y, Huxtable ST, Williams CB (2019) Impacts of process-induced porosity on material properties of copper made by binder jetting additive manufacturing. *Mater Des* 182:108001

**Publisher's Note** Springer Nature remains neutral with regard to jurisdictional claims in published maps and institutional affiliations.